PAPER J

RELATIVE ENTROPY ENHANCEMENT OF GEOPHYSICAL TOMOGRAPHY IMAGES

Gary Mavko

Seismic Tomography Project

ABSTRACT

Maximum Entropy (ME) and minimum Relative Entropy (RE) methods provide a powerful variational approach to extracting objective, high resolution images from incomplete and noisy data. They have proven useful for a wide variety of image reconstruction and enhancement problems in radio astronomy, spectral analysis, medical imaging, and photography. ME and RE have been widely applied to geophysical spectral analysis problems, but their application to geophysical seismic imaging is relatively new. A typical seismic image is underdetermined, so that an infinite number of images are consistent with the available data. Of that infinite number, the Maximum Entropy image is most objective and maximally non-committal with regard to the unknown information. The minimum Relative Entropy image is closest to a prior estimate of the image while still exactly consistent with the available partial information. In this paper ME and RE methods are applied to several synthetic images representative of those obtainable from cross-well seismic tomography. The two common forms of the entropy expression are compared, and while both lead to improved resolution, the "$-SlnS$" form was found to be more stable numerically. For the examples studied, ME enhancement slightly improved resolution compared to conventional Fourier reconstructions, but not nearly as much as the RE enhancement. An important innovation is the concept of weights applied to the prior estimate of the image. The weights express one's confidence in the prior estimate, and also allow the algorithm to "focus" on subsets of the image. In all examples, use of the weighting function gave improved resolution in the areas of interest.

INTRODUCTION

Geophysical tomography is an attempt to reconstruct an image of the subsurface from incomplete and noisy data. In the case of seismic diffraction tomography, seismic sources generate an incident wavefield which is scattered by velocity heterogeneities and sampled by receivers. Finite bandwidth, source and receiver geometry, and noise put fundamental limitations on the resolution of the reconstructed image.

A typical geometry for cross-well tomography is illustrated in Figure 1. A vertical array of sources lies within one well, and a vertical array of receivers lies within

a second well. A region of anomalous seismic velocity, $V(x,z)$, relative to a fairly uniform background, V_0, lies in between. The desired product of the tomographic inversion is an image of the anomalous velocity or the slowness $S(x,z) = 1./V(x,z)$.

It is equivalent to determine the Fourier transform, $\tilde{R}(k_x, k_z)$, of the slowness squared $S^2(x,y)$ for *all* spatial frequencies, k_x and k_z, since $S^2(x,z)$ can be recovered from $\tilde{R}$ by Fourier synthesis. Most of the popular geophysical diffraction tomography reconstruction algorithms (Devaney, 1984; Harris; 1987; Lo, 1987) are derived in the spatial frequency domain.

The problem is that only some of the Fourier components can be measured with realistic bandwidths and viewing angles. For a fixed $k = f/V_0$ (where f is the temporal frequency) and very long vertical source and receiver arrays, the most that can be sampled is a region of the (k_x, k_z) plane lying within the two semicircular disks shown in Figure 2. The radius of each disk is given by $k_{max} = f_{max}/V_0$, where f_{max} is the maximum temporal frequency recorded. It is clear from the plot that the vertical resolution will be much better than the horizontal resolution, because the coverage along the k_z axis is $\pm 2k_{max}$ and the coverage along the k_x axis is zero.

If the non-zero Fourier components of the desired object lie entirely within the sampled disks, then with good signal to noise and careful processing one might approach a near-perfect reconstruction of the image. However, if components lie outside of the sampled disks, then no amount of clever processing can recover them. The information is simply not measured.

In general, an infinite number of different images can be found whose Fourier transforms exactly match the measured transform within the sampled disks. Each choice corresponds to a different extension of the Fourier transform into the unsampled region. A common approach is to guess some particular extension, and the most common guess is that the unmeasured components are zero. This is built into virtually all conventional reconstruction techniques, including the direct Fourier reconstruction, the backprojection, and the filtered backpropagation techniques (Devaney, 1984; Harris, 1987, Lo, 1987).

The effect of zeroing regions of the (k_x, k_z) domain is illustrated in Figure 3. A synthetic slowness function representing three localized scatterers (anomalously slow material) superimposed on a uniform background is shown in Figure 3a. The separation between centers of the scatterers is 6 meters both vertically and horizontally. If we know all of the Fourier components of this object we can perfectly reconstruct it. If, however, we zero out all of the (k_x, k_z) domain that lies outside of the sampled disks shown in Figure 2b, we construct only a low-passed or narrow band version of the image, as shown in Figure 3b. For this example k_{max} corresponds to a minimum wavelength $\lambda_{min} = 1/k_{max} = 10.6$ meters. As expected, the low resolution image is blurred predominantly in the horizontal direction with the shallower two scatterers merged into a single broad ridge.

A second example is shown in Figure 4a. In this case, an anomalously slow horizontal layer is simulated, corresponding to high porosity sediments. In the middle of the layer a permeability barrier, corresponding to a loss of porosity, is simulated

by normal high velocity. The low resolution image, resulting from zeroing out all frequencies outside of the sampled disks, is shown in Figure 4b. In this example $\lambda_{min} = 1/k_{max} = 16$ meters. The sharp layer has become an easily recognizable rounded ridge, but the central anomaly is essentially gone with the loss of horizontal bandwidth.

A third example, shown in Figure 5a, is similar to the one in Figure 4a. In this case a very slow region is superimposed at the center of the slow layer. The corresponding low resolution image, resulting from zeroing out all frequencies outside of the sampled disks, is shown in Figure 5b. Again the central anomaly is essentially undetectable.

Part of the loss of resolution in these examples is a fundamental limitation of the experimental geometry, but part results from the rather specific and harsh assumption about the unknown Fourier components. We don't know the Fourier components outside of the disks, but for an arbitrary scatterer we can be fairly confident that those components are not equal to zero.

In contrast, Maximum Entropy (ME) and Relative Entropy (RE) methods (Jaynes, 1968; Burg, 1975; Shore and Johnson, 1980; Gull and Skilling, 1980; Gull and Skilling, 1984) use a variational approach to extend the partial information about the Fourier components in a physically more realistic way than assuming them to be zero. ME chooses the extension into the unsampled region that exactly incorporates all of the available information but is free of all other assumptions; RE chooses the extension that is closest to a prior estimate of the image, deviating only as necessary to satisfy the available measurements. In general, ME and RE enhanced images have higher resolution than conventional reconstructions while still agreeing exactly with the measured information. ME methods have been widely used for nongeophysical image processing (Wernecke and D'Addario, 1977; Skilling et al., 1979; Danielle and Gull, 1980; Gull and Skilling, 1984) and tomography (Lent, 1977; Mohammad-Djafari and Demoment, 1986). Both ME and RE enhancements have been applied to geophysical diffraction tomography by Lo (1987), but generally their use in geophysical tomography has been limited.

This paper illustrates and compares some of the features of ME and RE enhancement of images representative of cross-well diffraction tomography. We compare for several synthetic examples a conventional reconstruction with ME and RE enhanced reconstructions. A new feature is the incorporation of a weighting or confidence function applied to the prior estimate of the image. This is particularly useful for geophysical problems where the prior knowledge is good near boreholes and poor in the interwell region. ME has been shown to be useful for image enhancement when measurements are contaminated by noise and when the measurements are insufficient to uniquely determine the image. The discussion will be limited to the latter problem, specifically the bandwidth extrapolation and Fourier synthesis in cross-well situations. The starting point is to assume that some form of conventional reconstruction has been performed, so that the Fourier transform of the object is known within the sampled disks in the (k_x, k_z) plane. This bypasses the difficulties of the mapping or backpropagation from the receiver domain to the (k_x, k_z) domain, which

are discussed by Lo (1987).

MAXIMUM ENTROPY RECONSTRUCTION

Of the infinite number of images that agree exactly with the partial Fourier information, the one choice that is maximally non-committal with regard to the unknown information is the one that maximizes the entropy (Jaynes, 1968). Two common forms of the entropy expression have been applied to problems of spectral analysis and image enhancement, and a fairly extensive literature is devoted to debating the preferred one (Kikuchi and Soffer, 1977; Johnson and Shore, 1984; and Mohammad-Djafari and Demoment, 1986; Gull and Skilling, 1985).

The first approach treats the acoustic wavefield as a stationary random process similar to the application by Wernecke and D'Addario (1977) to electromagnet fields in radio astronomy. The desired slowness squared function, S^2, is then regarded as the a two dimensional (nonnegative) spectral density representative of the random field (Johnson and Shore, 1984; Mohammad-Djafari and Demoment, 1986). S^2 must be estimated from the 'autocorrelation' $\tilde{R}(k_x, k_z)$ of the wavefield, known only within the sampled disks in the (k_x, k_z) domain. This is precisely the spectral estimation problem treated by Burg (1975) and Mavko and Burg (1987). With this interpretation the entropy of the image has the form:

$$H_1 = \int_{-X}^{X} \int_{-Z}^{Z} lnS^2(x,z)dxdz \tag{1}$$

where X and Z are the dimensions of the image. The image that maximizes the entropy H_1 always has the functional form (Mavko and Burg, 1987):

$$S^2(x,z) = \frac{1}{\sum_{n,m} \lambda_{n,m} \exp\left(-i2\pi(xn\Delta k_x + zm\Delta k_z)\right)} \tag{2}$$

The unknown coefficients $\lambda_{n,m}$ correspond to the same spatial frequencies $(n\Delta k_x, m\Delta k_z)$ where the measurements of $\tilde{R}(n\Delta k_x, m\Delta k_z)$ are made, and the $\lambda_{n,m}$ are chosen to ensure that the image agrees with each of the Fourier measurements:

$$\int_{-X}^{X} \int_{-Z}^{Z} S^2(x,z) \exp\left(i2\pi(xr\Delta k_x + zs\Delta k_z)\right)dxdz = \tilde{R}(r\Delta k_x, s\Delta k_z) \tag{3}$$

It is assumed that the Fourier information $\tilde{R}$ can be found at or interpolated to an equally spaced rectangular grid within the sampled disks.

The second approach models the image itself $S^2(x,z)$, suitably normalized, as a probability density (Lo, 1987; Gull and Skilling, 1985). The entropy of the image in this case is given by:

$$H_2 = -\int_{-X}^{X} \int_{-Z}^{Z} S^2(x,z) lnS^2(x,z)dxdz \tag{4}$$

The image that maximizes the entropy H_2 always takes the form (see Appendix):

$$S^2(x,z) = \exp\left(-\alpha + \sum_{n,m} \lambda_{n,m} \exp\left(-i2\pi(xn\Delta k_x + zm\Delta k_z)\right)\right) \tag{5}$$

As before, the $\lambda_{n,m}$ are chosen to ensure that the image agrees with the Fourier measurements when S^2 is substituted into equation (3), and α is chosen to ensure the proper normalization for a probability density.

Maximum entropy enhancements of the blurred images in Figures 3b, 4b, and 5b are shown in Figures 3c, 4c, and 5c, using the H_2 entropy expression, equations (4) and (5). These were made by using a discrete approximation of (digitizing) the blurred images on a $1m \times 1m$ grid (32×64 samples) and fast Fourier transforming to obtain the known nonzero Fourier components $\tilde{R}(n\Delta k_x, m\Delta k_z)$ within the sampling disks. There were 135 "measured" components within the disks for the example in Figure 3, and 60 in Figures 4 and 5. The unknown coefficients $\lambda_{n,m}$ in the general form of the image $S^2(x,z)$ in equation (5) were found with a Newton-Raphson algorithm, similar to one suggested by Johnson(1983) for one dimensional problems and described in the Appendix. In all cases the ME images show slightly improved resolution, in both the vertical and horizontal directions, relative to the conventional reconstruction. In particular the two shallow scatterers in Figure 3c can begin to be resolved. The central anomalies in Figures 4c and 5c appear as a slight dip and peak, respectively, along the horizontal slowness ridge, but their "ringy" character makes them unconvincing and difficult to recognize as anomalies.

For comparison of the entropy forms H_1 and H_2, a ME enhancement of Figure 3b was also computed using the functional form for the image given by equation (2) and is plotted in Figure 3d. For this example there is little difference in the resolution performance of one form over the other, although the H_1 form is somewhat asymmetric in its estimate of the shallow peak amplitudes.

In general, the H_2 form appeared to be better behaved numerically than the H_1 form, at least using the Newton-Raphson algorithm. For both entropy forms, the resolution of the slowness image is improved by subtracting away most of the background average value $\Delta S^2 = S^2 - \alpha S_0^2$, where $0 < \alpha < 1$, treating the perturbation in slowness rather than the slowness itself. In terms of the scattering problem, only the perturbations in slowness are sources of the scattered field. When $\alpha = 1$ the perturbation is equivalent to the objective function $O(x,z) = 1 - S^2(x,z)/S_0^2$ that appears in the Born scattering theory. However, $O(x,z)$ can be negative, which violates both the spectral density and probability density interpretations of the image. Lo (1987) avoided that problem by treating the absolute value of $\mid O(x,z) \mid$, but this leaves an ambiguity in determining $\pm O(x,z)$. The effect of the background slowness on resolution is exactly the same as the effect of prewhitening in spectral estimation. The background numerically stabilizes or damps the problem, but at the expense of resolution. We found that the entropy form H_2 was stable with much less background damping, presumably because of the better behavior of H_2 as $S^2 \rightarrow 0$, compared with the behavior of H_1.

RELATIVE ENTROPY RECONSTRUCTION

Often in geophysical problems we have additional information in the form of a

prior velocity model that we wish to incorporate into the tomographic inversion. This prior information might come from well logs, surface seismic models, or geologic information. The relative entropy of an image $S^2(x,z)$ relative to a prior estimate of the image $P(x,z)$, again has two common interpretations. The first expresses the relative entropy between the unknown distribution of Fourier components of the wavefield and the prior distribution and leads to the following functional form (Johnson et al., 1984), analogous to equation (2):

$$S^2(x,z) = \frac{1}{\frac{1}{P(x,z)} + \sum_{n,m} \lambda_{n,m} \exp\left(-i2\pi(xn\Delta k_x + zm\Delta k_z)\right)} \tag{6}$$

The second approach is analogous to equation (4) and gives a relative entropy of the form:

$$H_2 = \int_{-X}^{X} \int_{-Z}^{Z} S^2(x,z) ln \frac{S^2(x,z)}{P(x,z)} dx dz \tag{7}$$

The image that minimizes H_2 always takes the form (see Appendix):

$$S^2(x,z) = P(x,z) \exp\left(-\alpha + \sum_{n,m} \lambda_{n,m} \exp\left(-i2\pi(xn\Delta k_x + zm\Delta k_z)\right)\right) \tag{8}$$

In both cases the unknown coefficients $\lambda_{n,m}$ must be found to ensure that the images agree exactly with the measurements $\tilde{R}(n\Delta k_x, m\Delta k_z)$, equation (3).

Relative entropy enhancements of the blurred images in Figures 4b and 5b are shown in Figures 4d and 5d. Only the H_2 forms are shown, again because of the superior numerical behavior compared with the H_1 form. In both cases the prior image $P(x,z)$ was chosen as a linear interpolation of the slowness at the wells – a uniform background slowness and the higher slowness layer without a center anomaly. In these images the prior has guided the image to give a very smooth background and a sharp edged layer. The additional information in the measurements $\tilde{R}(n\Delta k_x, m\Delta k_z)$ about the center anomalies causes a broad shallow dip in Figure 4d and a broad low peak in Figure 5d. Both central anomalies are more convincing and less ringy than in Figures 4c and 5c, although the width and magnitude of the anomalies are impossible to resolve.

RELATIVE ENTROPY WITH WEIGHTING

Situations will arise when the prior information is more reliable in some portions of the image, for example near the wells, than in other portions. In these cases one might wish to give a spatially variable weight to the prior, similar to the frequency dependent weight applied to one dimensional speech spectra by Johnson et al. (1984). Extending their result to two dimensions gives the following generalization of the H_1 form of entropy, equation (8):

$$S^2(x,z) = \frac{1}{\frac{1}{P(x,z)} + \frac{1}{W(x,z)} \sum_{n,m} \lambda_{n,m} \exp\left(-i2\pi(xn\Delta k_x + zm\Delta k_z)\right)} \tag{9}$$

where $W(x,z)$ is the weight function. Large values of W express a large confidence in the prior estimate. Arbitrary multiplicative factors on W do not affect the result, because they can be absorbed by the $\lambda_{n,m}$.

We write the alternative H_2 form of the weighted entropy as an extension of equation (9):

$$H_2 = \int_{-X}^{X} \int_{-Z}^{Z} W(x,z) S^2(x,z) ln \frac{S^2(x,z)}{P(x,z)} dx dz \tag{10}$$

The image that minimizes H_2 can be written as (see Appendix):

$$S^2(x,z) = P(x,z) \exp\left(-\alpha + \frac{1}{W(x,z)} \sum_{n,m} \lambda_{n,m} \exp\left(-i2\pi(xn\Delta k_x + zm\Delta k_z)\right)\right) \tag{11}$$

Weighted relative entropy enhancements of the images in Figures 4 and 5 are shown in Figures 4e and 5e. In both cases, the same prior was used as for Figures 4d and 5d. A broad, circularly symmetric Gaussian weighting function, $W(r) = 1 - .9\exp(-(r/12)^2)$, where $r = \sqrt{(x^2+z^2)}$, was centered on the layer, giving the center 10 times less confidence than the edges near the wells. While the prior generally guided the image, the low weight allowed the central anomalies to deviate from the prior. In both cases the result is a narrower, better resolved central anomaly.

A similar weighting strategy was applied to the blurred image in Figures 3b. In this case we observe the narrow deep peak and the broad shallower one. We choose a prior that is uniform everywhere except for a single deep localized scatterer. Since we are uncertain about the shallower ridge we choose a broad weighting function $W(x,z) = 1. - .9\exp(-(x/12)^2 - (z/3)^2)$, centered on the shallow anomaly that weights it 10 times less than the rest of the image. The result is shown in Figure 3e, and has marked improvement in resolution of the two peaks.

DISCUSSION

Variational techniques provide a useful way of improving and stabilizing image reconstruction in problems with incomplete and noisy data. Common approaches are to choose the image that has, for example, the minimum energy (Devaney, 1984) or that is in some way the smoothest. The maximum entropy image is the one that is most objective, containing no more information than is actually in the limited measurements of the image. Relative entropy methods provide an objective way of incorporating prior information into the reconstruction. The RE image deviates from the prior no more than is necessary to satisfy the measured constaints.

ME and RE methods have been widely applied to problems in radio astronomy (Wernecke and D'Addario, 1977; Gull and Skilling, 1984) and spectral analysis (Burg, 1975; Mavko and Burg, 1987). Lo (1987) applied relative entropy to geophysical tomographic images reconstructed from laboratory measurements on physical models.

In this paper we compare the two common entropy forms, the "lnX" and the "$-XlnX$". Although the "lnX" is often superior for spectral analysis of both one-dimensional and two-dimensional problems, the $-XlnX$ is usually favored in image

inhancement. Experiments here favor the latter form, because of slightly better resolution, but mostly because of better numerical stability.

The most important new point here is the introduction of a spatially dependent weighting function applied to the prior estimate. This is particularly valuable in cross-well tomography problems where information about the prior is heterogeneous – high confidence near the wells and in clean data areas, but low elsewhere. Low weights also seem to focus the algorithm for improved resolution in areas of low weight. In examples 3e, 4e, and 5e, the low weight features were resolved better than before.

APPENDIX

We wish to minimize the entropy, H_2, which is written in the form:

$$H_2 = \int_{-X}^{X} \int_{-Z}^{Z} W(x,z) Q(x,z) ln \frac{Q(x,z)}{P(x,z)} dx dz \tag{12}$$

where $Q(x,z)$ is the image, $P(x,z)$ is the prior estimate of the image, and $W(x,z)$ is the positive weighting function on the prior. We know that $Q(x,z)$ can be written in terms of its Fourier transform, $\tilde{R}(n\Delta k_x, m\Delta k_z)$, which for shorthand we write as $R_{n,m}$.

$$Q(x,z) = \sum_{n=-\infty}^{\infty} \sum_{m=-\infty}^{\infty} R_{n,m} \exp\left(-i2\pi(xn\Delta k_x + zm\Delta k_z)\right) \tag{13}$$

However, only a small finite number of the $R_{n,m}$ are known. From equation (13) we see that

$$\frac{\partial Q}{\partial R_{n,m}} = \exp\left(-i2\pi(xn\Delta k_x + zm\Delta k_z)\right) \tag{14}$$

Using equation (14) we minimize H_2 with respect to the unknown $R_{n,m}$ by setting the derivatives equal to zero:

$$\frac{\partial H_2}{\partial R_{n,m}} = \int_{-X}^{X} \int_{-Z}^{Z} W(x,z)[1 + ln \frac{Q(x,z)}{P(x,z)}] \exp\left(-i2\pi(xn\Delta k_x + zm\Delta k_z)\right) dx dz = 0 \tag{15}$$

Now, assuming the integrand is a smooth, well behaved function, it can be written in terms of its Fourier coefficients $\lambda_{r,s}$:

$$W(x,z)[1 + ln \frac{Q(x,z)}{P(x,z)}] = \sum_{r=-\infty}^{\infty} \sum_{s=-\infty}^{\infty} \lambda_{r,s} \exp\left(-i2\pi(xr\Delta k_x + zs\Delta k_z)\right) \tag{16}$$

Now substituting equation (16) into equation (15) we get

$$\sum_{r=-\infty}^{\infty} \sum_{s=-\infty}^{\infty} \lambda_{r,s} \int_{-X}^{X} \int_{-Z}^{Z} \exp\left(i2\pi(x(n-r)\Delta k_x + z(m-s)\Delta k_z)\right) dx dz = 0 \tag{17}$$

which leads us to the conclusion that $\lambda_{r,s} = 0$ when $r = -n$ and $s = -m$. The $\lambda_{r,s}$ are nonzero only for the (n,m) where measurements are available. Now solving equation

(16) for Q, and using only the nonzero $\lambda_{r,s}$:

$$Q(x,z) = P(x,z)\exp\left(-\alpha + \frac{1}{W(x,z)}\sum_{r,s}\lambda_{r,s}\exp\left(-i2\pi(xr\Delta k_x + zs\Delta k_z)\right)\right) \quad (18)$$

which is the same as equation (11). The parameter α represents the scaling parameter that must be used for the additional constraint that $\int\int Q dx dz = 1$. Setting the weighting function $W(x,z) = 1$ gives equation (8) and setting both $W(x,z) = 1$ and $P(x,z) = 1$ gives equation (5).

For the Newton-Raphson algorithm we need to evaluate the derivatives $\partial R_{n,m}/\partial\lambda_{r,s}$. Begin with

$$R_{n,m} = \int_{-X}^{X}\int_{-Z}^{Z} Q(x,z)\exp\left(i2\pi(xn\Delta k_x + zm\Delta k_z)\right)dxdz \quad (19)$$

$$\frac{\partial R_{n,m}}{\partial\lambda_{r,s}} = \int_{-X}^{X}\int_{-Z}^{Z}\frac{\partial Q(x,z)}{\partial\lambda_{r,s}}\exp\left(i2\pi(xn\Delta k_x + zm\Delta k_z)\right)dxdz \quad (20)$$

Substituting $\partial Q/\partial\lambda$ from equation (18) allows us to write

$$\frac{\partial R_{n,m}}{\partial\lambda_{r,s}} = \int_{-X}^{X}\int_{-Z}^{Z}\frac{Q(x,z)}{W(x,z)}\exp\left(i2\pi(x(n-r)\Delta k_x + z(m-s)\Delta k_z)\right)dxdz \quad (21)$$

The Newton-Raphson algorithm begins with an initial guess of the unknown $\lambda_{r,s}$ which are substituted into equations (18) to evaluate the corresponding estimate of Q. The Fourier sum in equation (18) is conveniently evaluated with a two-dimensional FFT. The corresponding autocorrelation is evaluated from equation (19) approximated with a two-dimensional FFT. The misfit $\Delta R_{n,m}$ with the measured autocorrelation is used to compute corrections $\Delta\lambda_{r,s}$ using the matrix of derivatives in equation (21). Note that the derivatives are also easily computed by taking an FFT of $Q(x,z)/W(x,z)$ and selecting the terms $(n-r, m-s)$.

REFERENCES

Burg, J.P., 1975, Maximum entropy spectral analysis, Ph.D. dissertation, Stanford University, Stanford, California.

Danielle, G.J. and Gull, S.F., 1980, Maximum entropy algorithm applied to image enhancement, IEE Proceedings, Pt. E., 127, 170-172.

Devaney, A.J., 1984, Geophysical diffraction tomography, IEEE Trans. Geoscience and Remote Sensing, GE-22, 3-13.

Gull, S.F. and Skilling, J., 1984, Maximum entropy method in image processing, IEE Proceedings, Pt. F, 131, 646-659.

Gull, S.F. and Skilling, J., 1985, The entropy of an image, in Maximum Entropy and Bayesian Methods in Inverse Problems, Reidel Pub. Co., Dordrecht.

Harris, J.M., 1987, Diffraction tomography with arrays of discrete sources and receivers, IEEE Trans. Geoscience and Remote Sensing, GE-25, 448-455.

Jaynes, E.T., 1968, Prior probabilities, IEEE Trans. Sys. Sci. and Cyber., SSC-4, 227-241.

Johnson, R.W., 1983, Algorithms for single-signal and multisignal minimum-cross-entropy spectrum analysis, NRL Report 8667, Naval Research Lab, Washington, D.C.

Johnson, R.W. and Shore, J.E., 1984, Which is the better entropy expression for speech processing: -S log S or log S?, IEEE Trans. Acoust., Speech, and Sig. Proc., ASSP-32, 129-137.

Johnson, R.W., Shore, J.E., and , J.P., 1984, Multisignal minimum-cross-entropy spectrum analysis with weighted initial estimates, IEEE Trans. Acoust. Speech, and Sig. Proc., ASSP-32, 531-539

Kikuchi, R. and Soffer, B.H., 1977, Maximum entropy image restoration. I. The entropy expression, J. Opt. Soc. Am., 67, 1656-1665.

Lent, A., 1977, A convergent algorithm for maximum entropy image restoration, with a medical X-ray application: Image analysis and evaluation, SPSE Conv. Proc., R. W. Shaw, Ed., Washington, D.C., Soc. Photogr. Sce. Eng., 249-257.

Lo, T-W., 1987, Seismic borehole tomography, Ph.D. dissertation, Massachusetts Institute of Technology.

Mavko, G.M. and Burg, J.P., 1987, Two-dimensional maximum entropy spectral analysis, Presented at SEG 57th Annual Meeting, New Orleans.

Mohammad-Djafari, A. and Demoment, G., 1986, Maximum entropy diffraction tomography, 1968, IEEE ICASSP 86 Tokyo, 1749-1752.

Shore, J.E. and Johnson, R.W., 1980, Axiomatic derivation of the principle of maximum entropy and the principle of minimum cross-entropy, 1980, IEEE Trans. Inf. Theory, IT-26, 26-943.

Skilling, J., Strong, A.W., and Bennet, K, 1979, Maximum-entropy image processing gamma-ray astonomy, Mon. Not. R. ast. Soc. 145-152.

Wernecke, S.J. and D'Addario, L.R., 1977, Maximum entropy image reconstruction, IEEE Trans. Computers, C-26, 351-364.

Borehole tomography

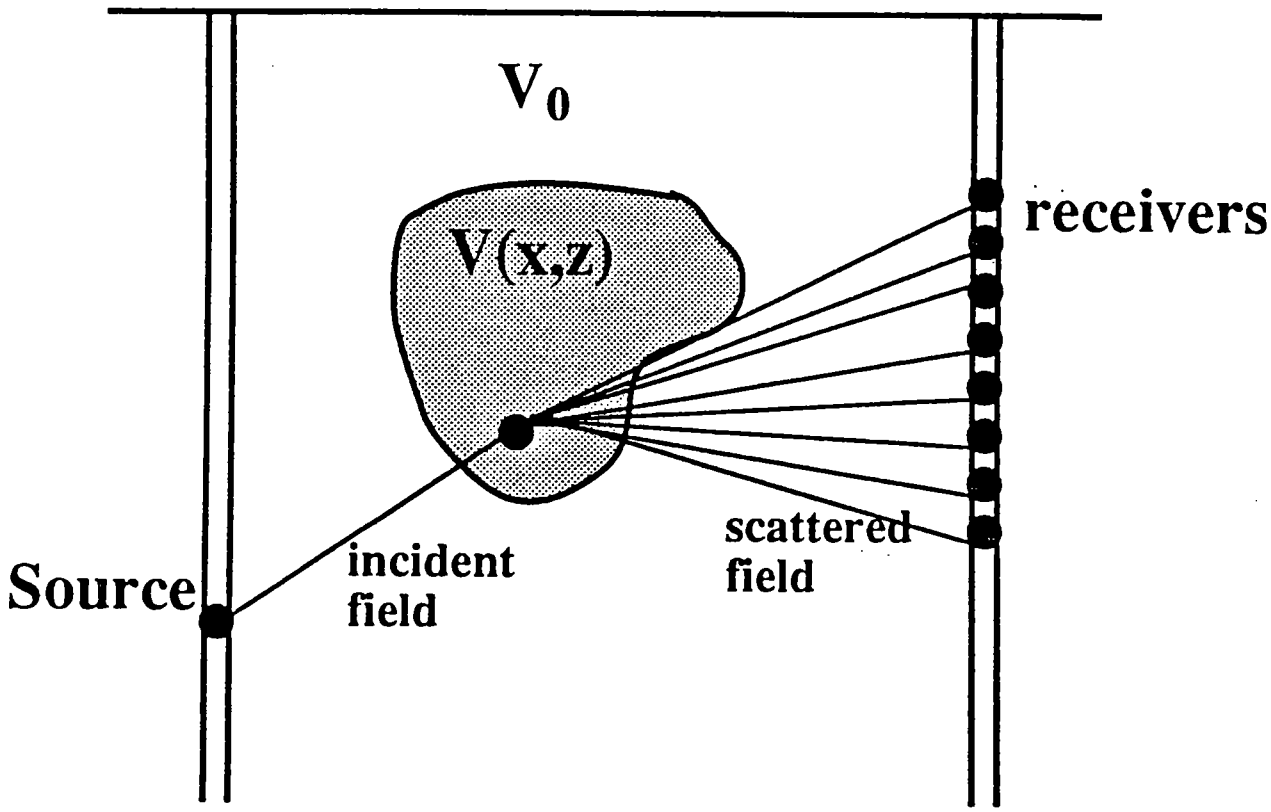

Figure 1: Typical crosswell survey geometry, in which we wish to image the velocity field V(x,z).

Limited Sampling in k-k domain

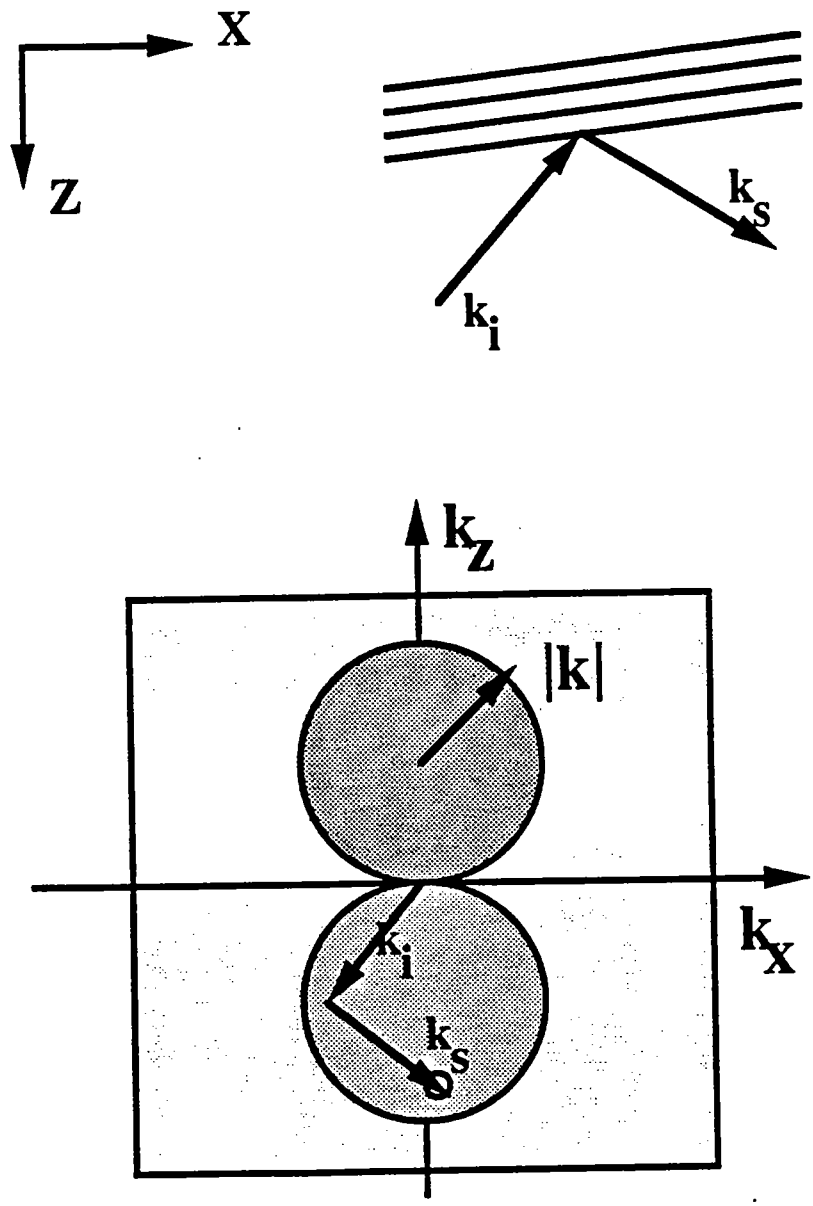

Figure 2: Only certain Fourier components of the desired image can be measured in a diffraction tomography experiment. For the crosswell geometry these components are limited to two circular disks as shown.

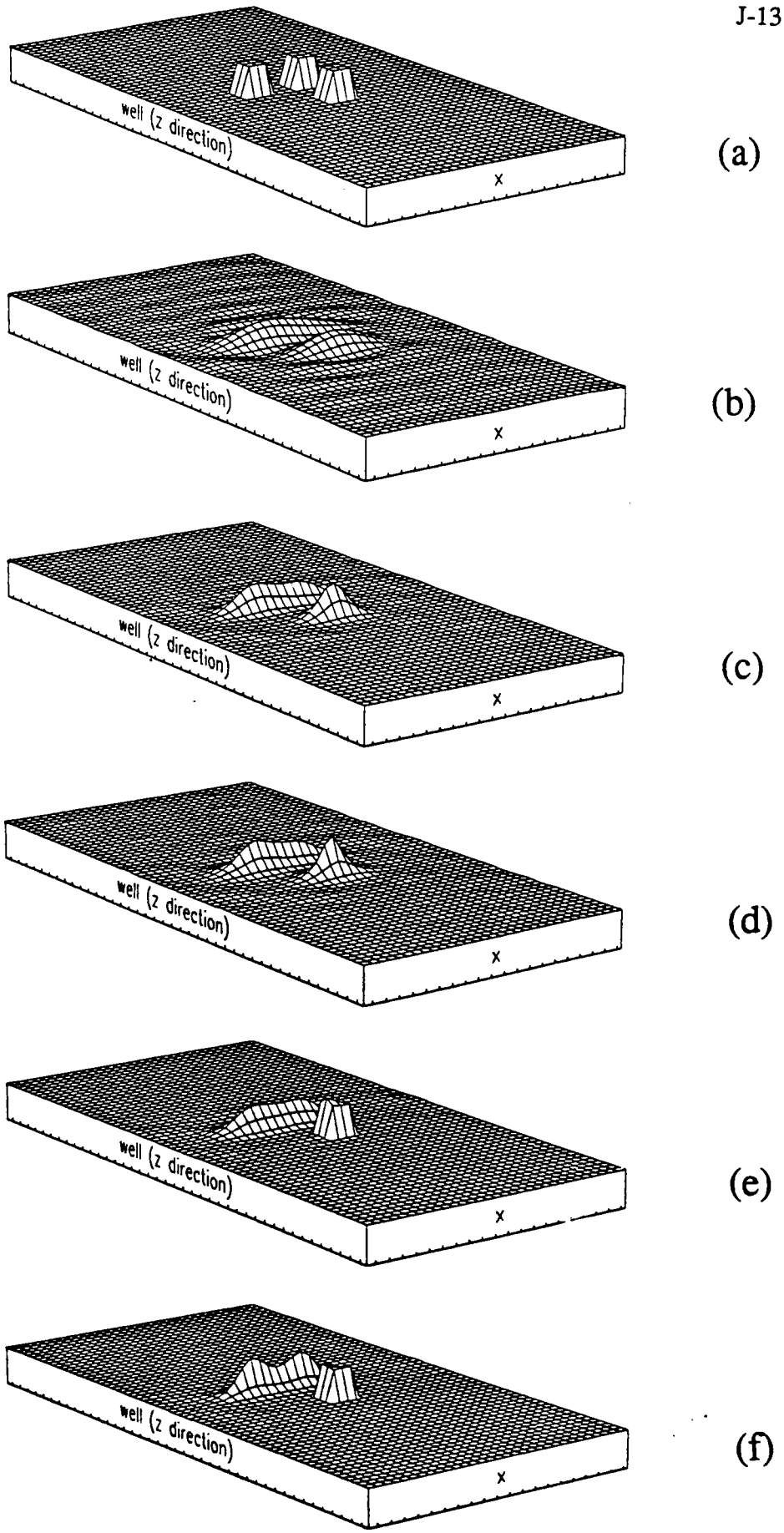

Figure 3: (a) Three scatterers. (b) Result of zeroing the unknown components. (c)-(d) ME enhancements. (e) RE enhancement with the deeper scatterer in the prior. (f) RE enhancement when the shallow anomaly is given a very low weight.

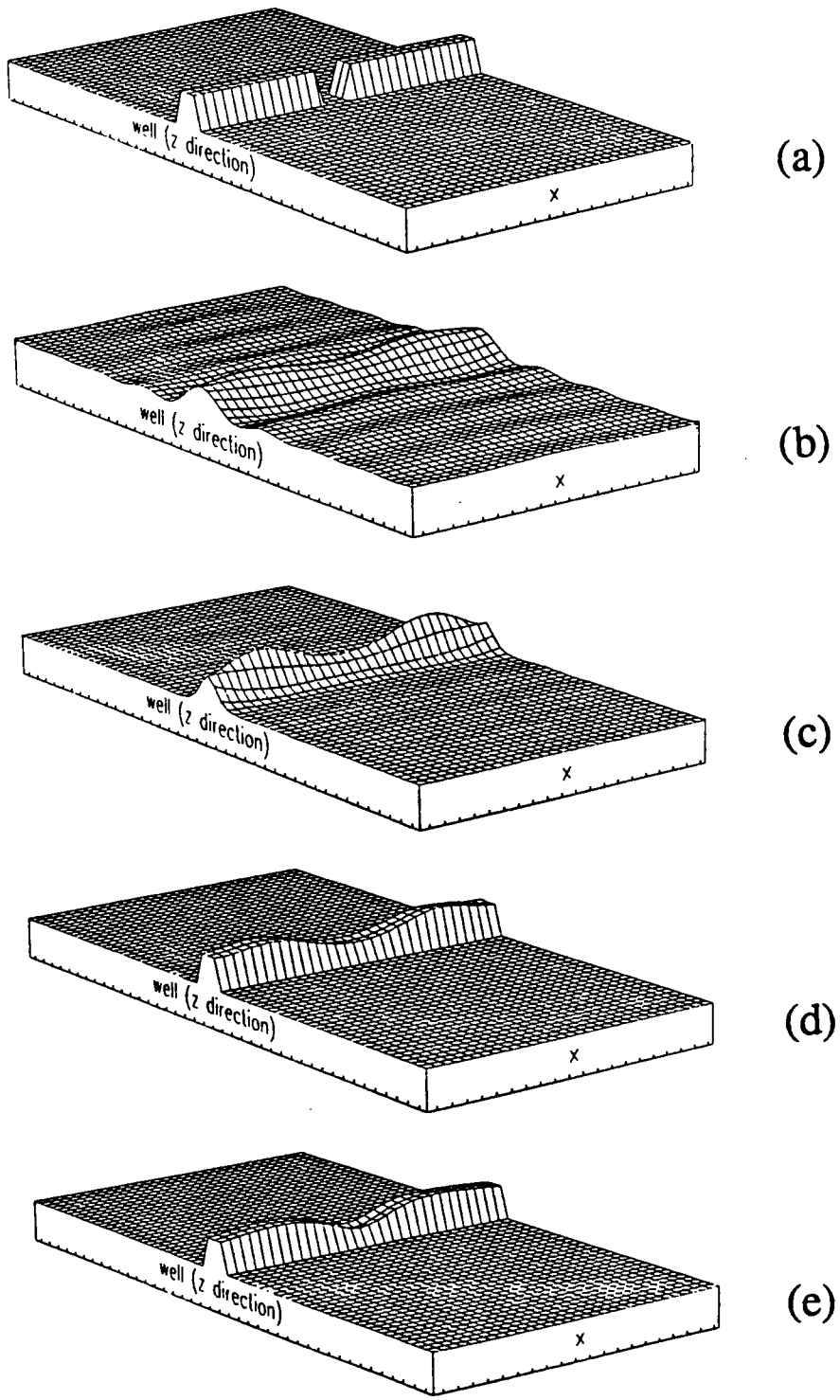

Figure 4: (a) A synthetic slow horizontal layer with a permeability barrier. (b) Result of zeroing out the unsampled components. (c) ME enhancement. (d) RE enhancement with a uniform layer as the prior. (e) Very low weight given to the region between the wells.

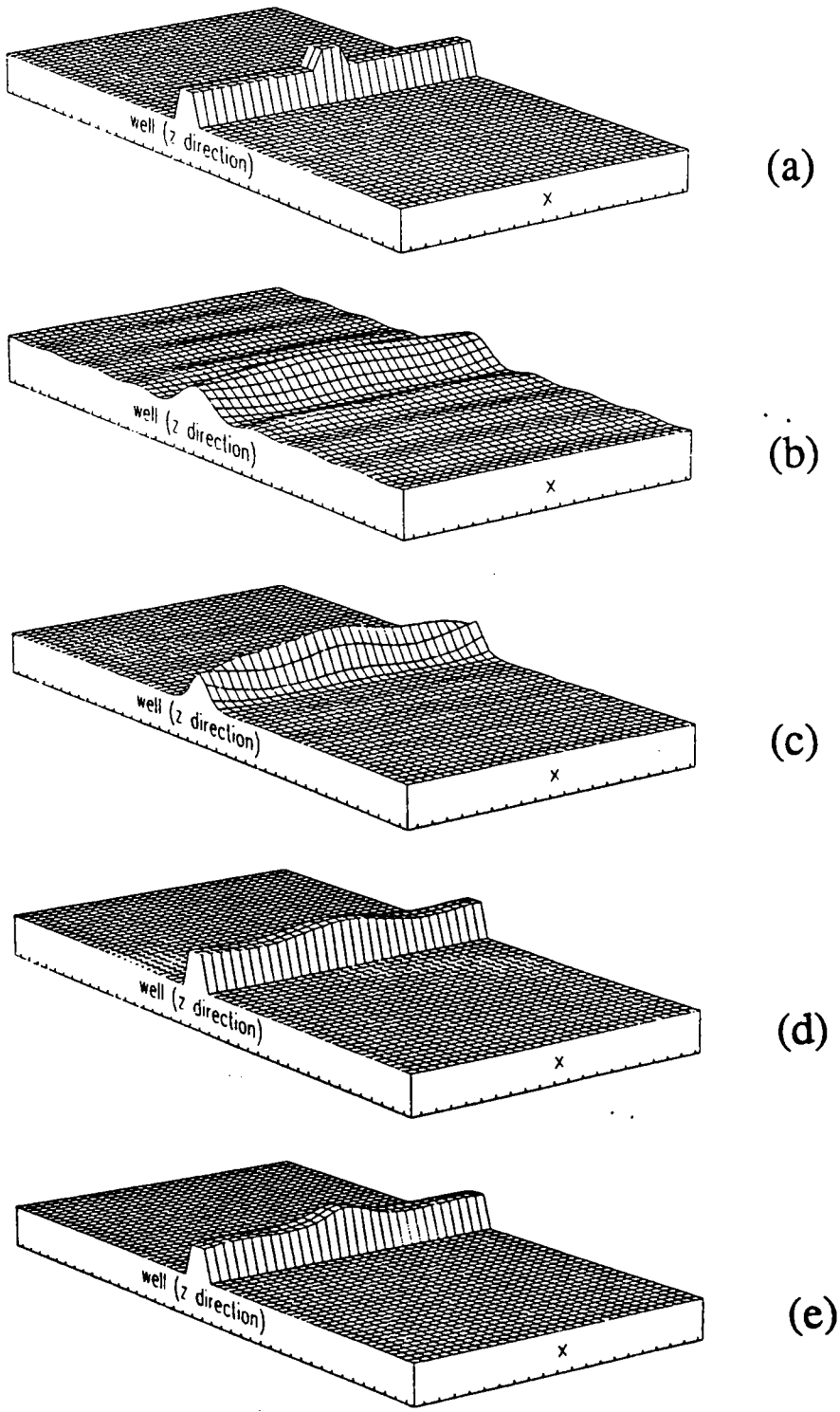

Figure 5: Similar to Figure 4 with the central anomaly slower instead of faster.